SUPPLEMENTARY MATERIAL:

Simulation of multiple ion channel block provides improved prediction of compounds' clinical torsadogenic risk

Gary R. Mirams, Yi Cui, Anna Sher, Martin Fink, Jonathan Cooper,
Bronagh M. Heath, Nick C. McMahon, David J. Gavaghan, Denis Noble.

January 31, 2011

Contents

1 Experimental Protocols **2**

2 Simulation Protocols **4**

3 Details of Statistical Methods **6**

3.1 Linear Discriminant Analysis Implementation 6

3.2 Cross-validation 7

4 Most predictive markers **13**

5 Classification Errors **14**

6 Full list of references **15**

1 Experimental Protocols

For the I_{Na} experiments HEK-293 cells stably transfected with hNaV1.5 cDNA were continuously maintained in a humidified, gassed (∼5% CO_2) incubator at approximately 37℃, and passaged using Dulbecco's Modified Eagle Medium (DMEM) supplemented with 10% foetal bovine serum, 1% non-essential amino acids, 1% penicillin/streptomycin and 0.4 mg/mL geneticin. For the I_{CaL} experiments myocytes were isolated enzymatically from guinea-pig ventricle as previously described[21]. Briefly, male guinea-pigs were killed by cervical dislocation following stunning. Myocytes were isolated after perfusion of the heart with a physiological salt solution containing reduced calcium and 0.8 mg/mL of collagenase Type 1 (Worthington Biochemicals). Cells were stored at room temperature in Dulbecco's MEM (Life Technologies, Scotland) and used for electrophysiological investigation on the day of preparation. For the I_{Kr} experiments HEK-293 cells stably transfected with hERG cDNA were obtained from the University of Wisconsin. The cells were continuously maintained in, and passaged, using minimum essential medium supplemented with 10% foetal bovine serum, 1% non-essential amino acids, 1% sodium pyruvate, 1% penicillin/Streptomycin and 0.4 mg/ml geneticin. The cells were seeded onto glass coverslips in 35 mm^2 dishes (containing 3 ml medium without geneticin) at a density that enabled isolated cells to be selected for patch-clamping.

The conventional whole-cell patch-clamp configuration was used to record membrane currents at room temperature via AxoPatch 200B preamplifiers, and data acquisition and analysis were controlled by Axon pClamp software.

For the I_{CaL} experiments, the composition of the bath solution was (in mM): NaCl 125; NaHCO3 25; KCl 5.4; $CaCl_2$ 1.8; $MgCl_2$ 1.0; NaH_2PO_4 1.2; D-glucose 5.5; CsCl 5.0; pH 7.4 when bubbled with 95% O_2 and 5% CO_2; the composition of the pipette solution was (mM): CsCl 120; TEACl 20; $MgCl_2$ 5.5; EGTA 5.0; ATP-Na2 5.0, HEPES 20; phosphocreatine 5.0; pH 7.2 with 1M CsOH.

For the I_{Na} experiments, the composition of the bath solution was (mM): NaCl 40; CsCl 97; KCl 4.0, $CaCl_2$ 1.8; $MgCl_2$ 1.0; D-glucose 10; HEPES 10; pH 7.4 with 1M CsOH; the composition of the pipette solution was (mM): CsCl 130; $MgCl_2$ 5.0; EGTA 5.0; MgATP 4.0; GTP 0.1, HEPES 10; pH 7.2 with 1M CsOH.

The voltage protocols for studying the concentration-dependent effect of the compounds on peak current were as follows. For I_{Na}, a step from −100 mV (holding potential) to −30 mV for 20 ms, then step back to a holding potential of −100 mV. For I_{CaL}, a step from −40 mV (holding potential) to 0 mV for 400 ms, and then stepped back to the holding potential of −40 mV. The pulses were applied at frequencies of 0.1 and 0.2 Hz for I_{Na} and I_{CaL} respectively. Peak I_{Na} was measured with respect to the holding current measured at −100 mV just before the step depolarisation and peak I_{CaL} amplitude was measured relative to the holding current at −40 mV. For I_{Kr}, the holding potential was −80 mV. The step from −80 mV to the test command (+20 mV, 5 s) activated hERG channels and the step from the test command (+20 mV) to −50 mV (5 s) resulted in the tail current, whose amplitude was measured. The testing pulses were applied at 15 s intervals. These protocols were used to construct concentration-response curves.

Experiments were performed at Safety Pharmacology, GlaxoSmithKline. The investigation conforms with the Guide for the Care and Use of Laboratory Animals published by the US National Institutes of Health (NIH Publication No. 85-23, revised 1996). All animals were treated in accordance with UK Home Office regulations (Animals (Scientific Procedures) Act 1986: London: Her Majesty's Stationery Office 1986) and the work was approved by internal ethical review.

2 Simulation Protocols

In this section we describe the three protocols under which the models were used to simulate cellular responses, and state the model outputs that we have taken as potential *in-silico* risk indicators. We correlated these markers against the TdP risk categories as described in section 2.4 of the main text and section 3.1 of this document, in order to establish those markers that provided an indication of risk.

Firstly, we considered the membrane voltage under regular pacing. Models were paced at 1Hz for 1000 seconds in order to obtain an approximately steady behaviour. The final AP was analysed and the maximum upstroke velocity (proportional to peak current), peak membrane voltage, and APD at 50% and 90% repolarisation were recorded, along with APD90 minus APD50 as measure of 'triangulation'. The cytosolic calcium transient corresponding to this AP was also analysed; peak calcium, 50% duration, 90% duration and triangulation of the transient were recorded.

Secondly, the S1-S2 restitution protocol, was performed on the models. 1Hz was chosen as the S1 pacing frequency and the models were again paced for 1000 seconds in order to obtain a steady state before the protocol began. Results were analysed to determine the maximum slope of the restitution curve.

Finally, a dynamic restitution protocol was performed. This consisted of 100 paces at varying frequencies from 1Hz up to 10Hz. The final eight action-potential traces at each frequency were analysed to detect voltage alternans and the frequency at which depolarisation occurred before 90% repolarisation had completed (i.e. the frequency at which non-spontaneous EADs were induced), the highest pacing cycle length at which either occurred was recorded as the 'instability onset'. The maximum slope of the dynamic restitution curve was recorded. The area between the control and drug-blocked dynamic restitution curves was also recorded; this measure is intended to quantify the change in APD over a range of pacing frequencies.

The full list of the 15 simulated markers is:

1. Steady-State 1Hz pacing
    - APD90
    - APD50
    - APD Triangulation
    - Peak membrane voltage
    - Maximum upstroke velocity
    - Ca duration 90
    - Ca duration 50
    - Ca triangulation
    - Peak Ca

2. S1-S2 Restitution
    - Maximum slope
3. Dynamic Restitution
    - Maximum slope
    - Alternans onset pacing frequency
    - (non-spontaneous) EAD onset frequency
    - Instability onset frequency
    - Area between control and drug curves

The tolerances of CVODE were set as: relative, 10^{-5}; absolute, 10^{-7}. The simulations involved in determining the 1Hz APD90 for the Grandi *et al.* model for a compound at a particular concentration, and the subsequent classification of the compound into a risk category, can be completed in under one minute on a single core of a desktop PC (an Intel Core2 Duo 3GHz desktop PC was used). We propose that the calculation be performed for a range of concentrations, informing the therapeutic doses at which the compound may be used safely.

3 Details of Statistical Methods

In this section we provide more details on the statistical methods used to evaluate the predictive power of the different markers. Section 3.1 provides details of the implementation of the LDA technique, and section 3.2 provides details of validation techniques used to ensure that the predictive power of our markers was not down to chance.

3.1 Linear Discriminant Analysis Implementation

We assemble a large matrix of training data $\mathbf{X}$ from distinct categories $k = 1 \dots K$ (in our case $K = 4$ — the number of risk categories after combining 1 and 2 due to their equal risk). Each row i of $\mathbf{X}$ represents a drug, and each column j contains a 'discriminant variable' — one of our measures (e.g. hERG IC50 or simulated APD90 from a particular model). Here we follow the notation of Hastie *et al.* [80], to whom we refer the interested reader to their section 4.3 for a full derivation of this technique.

Our prior distributions (the likelihood that a drug belongs to a particular category) are set equal and given as

$$\pi_k = 1/K, \tag{1}$$

If the mean value of our measures for the training points in category k is denoted by the vector μ_k, then the 'pooled' or 'common' covariance matrix is given by

$$\mathbf{\Sigma} = \sum_{k=1}^{K} \sum_{\forall i \in k} \left(\mathbf{X}_i - \mu_k\right) \left(\mathbf{X}_i - \mu_k\right)^T / \left(N - K\right). \tag{2}$$

where N is the total number of drugs and $\mathbf{X}_i$ is a vector of measures for a particular drug. The linear discriminant functions for each category are then given by

$$\delta_k(y) = y^T \mathbf{\Sigma}^{-1} \mu_k - \frac{1}{2} \mu_k^T \mathbf{\Sigma}^{-1} \mu_k + \ln\, \pi_k. \tag{3}$$

A new observation y is then classified to the category k for which the discriminant function $\delta_k(y)$ is largest. Notice that for the 1D markers presented in the main text $\mathbf{X}_k$ is a column vector. We demonstrate briefly how this method works in Figure S1.

In the bottom panel of Figure S1 we see a set of training data from four distinct categories, distributed along a one dimensional variable 'y'. LDA is derived based on the assumption that the training data in each category are normally distributed, with each category having a different mean but a common covariance matrix. Our dataset is not large enough to test whether the points in each category follow a normal distribution, yet in practice LDA has been found to work well for many distributions [80]. LDA then uses maximum likelihood estimates to calculate the probability of each point in y-space being a member of each category. The resulting probability of an unseen observation belonging to each of the categories is shown in the top panel of Figure S1. To classify an unseen observation we simply assign it to the category with the highest probability at that point.

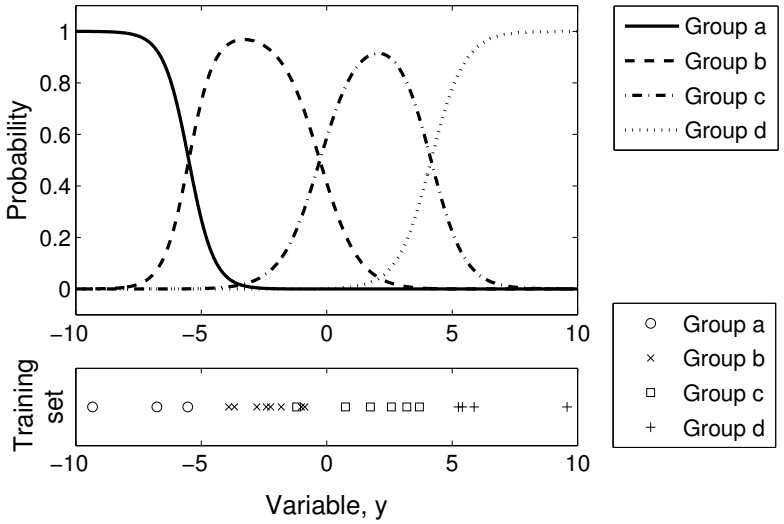

Figure S1: An example of how linear discriminant analysis classifies points in variable space into distinct categories. Bottom: a set of 1D training variables taken from four distinct categories. Top: the probability of being classified into each category at each point in (1D) variable space, each point in variable space would be classified into the category k with the largest discriminant function $\delta_k(y)$ (or equivalently probability) at that point.

3.2 Cross-validation

Despite the fact that the errors in classification as shown in Figure 4 of the main text are entirely independent of the training data (because of the N-fold cross validation/'leave-one-out validation'), a possible criticism of our approach would be that we tried many different markers, and the success of the best-performing one was purely by chance. We have evaluated the predictive power that such 'random guesses' for the categories would provide. In Figure S2 we plot the resulting error for 1,000; 10,000; 100,000 and 1,000,000 random guesses: none of the resulting errors are as small as those of the simulated marker suggested in the main text. This finding suggests that the measure has strong predictive power and has not been successful 'by chance'.

The fact that the distribution shown in Figure 5 in the main text shows a clear bias towards "being predictive", rather than "being random" (as plotted in Figure S2) provides further evidence that our approach is indeed producing predictive power and our findings are not a chance result. Indeed the 30 "most predictive" markers listed in Supplementary Material 4, and shown in bold on Figure 5 of the main text, are all multi-channel markers. None of the hERG-only markers were as accurate, providing further evidence that the multichannel simulations are not outperforming the existing measures by chance.

Yet, we acknowledge that the choice of best marker was strongly dependent on the dataset. In order to ascertain whether our measure of Grandi *et al.*[26] APD90 was robust to the different datasets of drugs we split them into separate groups for K-fold cross validation of the marker choice. Although Hastie *et al.*[80] suggest that K is

generally taken to be between 5 and 10 we use $K = 4$ because we only have four drugs in category 2.

1. Quinidine (1), Ajmaline (1), Cisapride (2), Pimozide (3), Fluvoxamine (4), Mibefradil (4), Risperidone (5), Nitrendipine (5).

2. Amiodarone (1), Terfenadine (2), Sertindole (3), Bepridil (3), Desipramine (4), Amitryptyline (4), Nifedipine (4), Cibenzoline (5), Verapamil (5).

3. Dofetilide (1), Prenylamine (2), Chlorpromazine (3), Diphenhydramine (4), Imipramine (4), Phenytoin (5), Propranolol (5).

4. Tedisamil (1), Thioridazine (2), Haloperidol (3), Propafenone (4), Mexiletine (4), Quetiapine (4), Diltiazem (5).

These groups were chosen so that each contained roughly equal numbers of drugs from each of the risk categories (as shown in brackets after the drug name). The stratified training datasets were then formed by 'leave-one-group-out': so stratification set 1 was formed from groups $2, 3, 4$, stratification set 2 from groups $1, 3, 4$ etc. This was necessary to ensure that each risk category contained a number of points with which to 'train' the LDA method.

The method referred to in the main text (individual 'leave-one-out' for each compound, LDA, and finally classification) was then performed for each of these stratified training datasets. We subsequently ranked the predictive power of each marker in each of the training datasets.

In Figure S3 we present the same data as in the main text's Figure 5 for each of the stratified datasets. The top 30 markers for the full dataset are again shown in bold. We see that the most predictive measures are relatively robust across the different stratifications, and in particular our best measure Grandi *et al.*[26] APD90 as designated by the dotted lines) consistently outperforms both the existing measure (dashed lines) and random guesses (solid lines).

In addition to the experiment displayed in the main text we also performed a 2D LDA analysis for every combination of the 761 1D markers (289180 in total). The result of this was a slight improvement over the 1D markers (as shown in Figure S4), but a possible loss of consistency between stratified groups as shown in Figure S5 (it is possible that out of so many markers "predictive" ones appear by chance, as shown in Figure 2(c) for 100,000 random category guesses). For this reason the main text refers only to the more robust 1D markers.

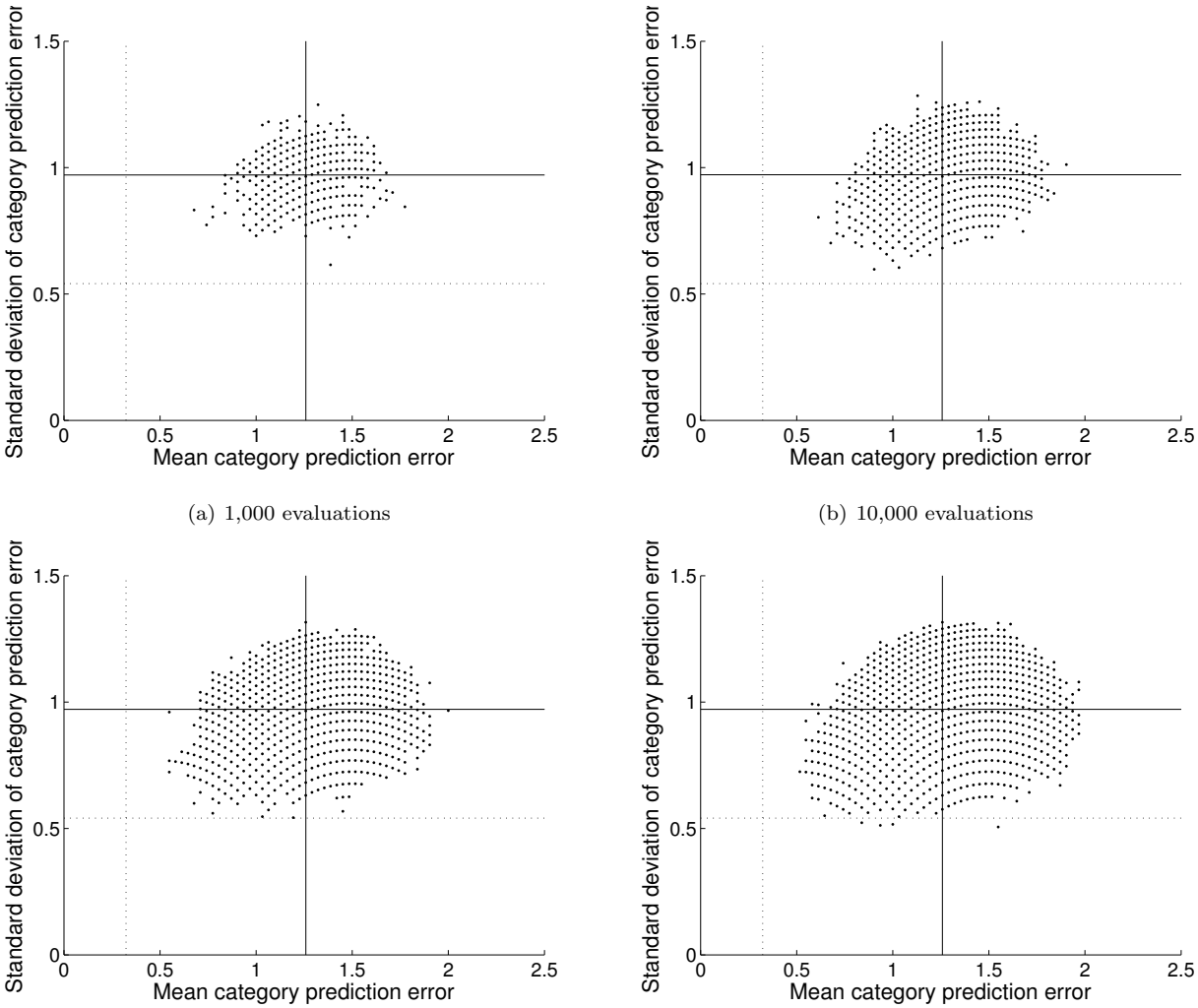

(a) 1,000 evaluations

(b) 10,000 evaluations

(c) 100,000 evaluations

(d) 1,000,000 evaluations

Figure S2: Classification errors resulting from (a) $1,000$; (b) $10,000$; (c) $100,000$; and (d) $1,000,000$ sets of random guesses for the drug risk categories. The mean values on each plot are given by solid lines, and the errors given by the 1D simulated marker (Figure 5 in the main text) are shown by dashed lines. It appears that categorisation at random has far less than 1 in a million chance of performing as well as the simulated marker. The 'patterns' arise because there are a limited number of possible mean and standard deviations in errors with a fixed number of drugs.

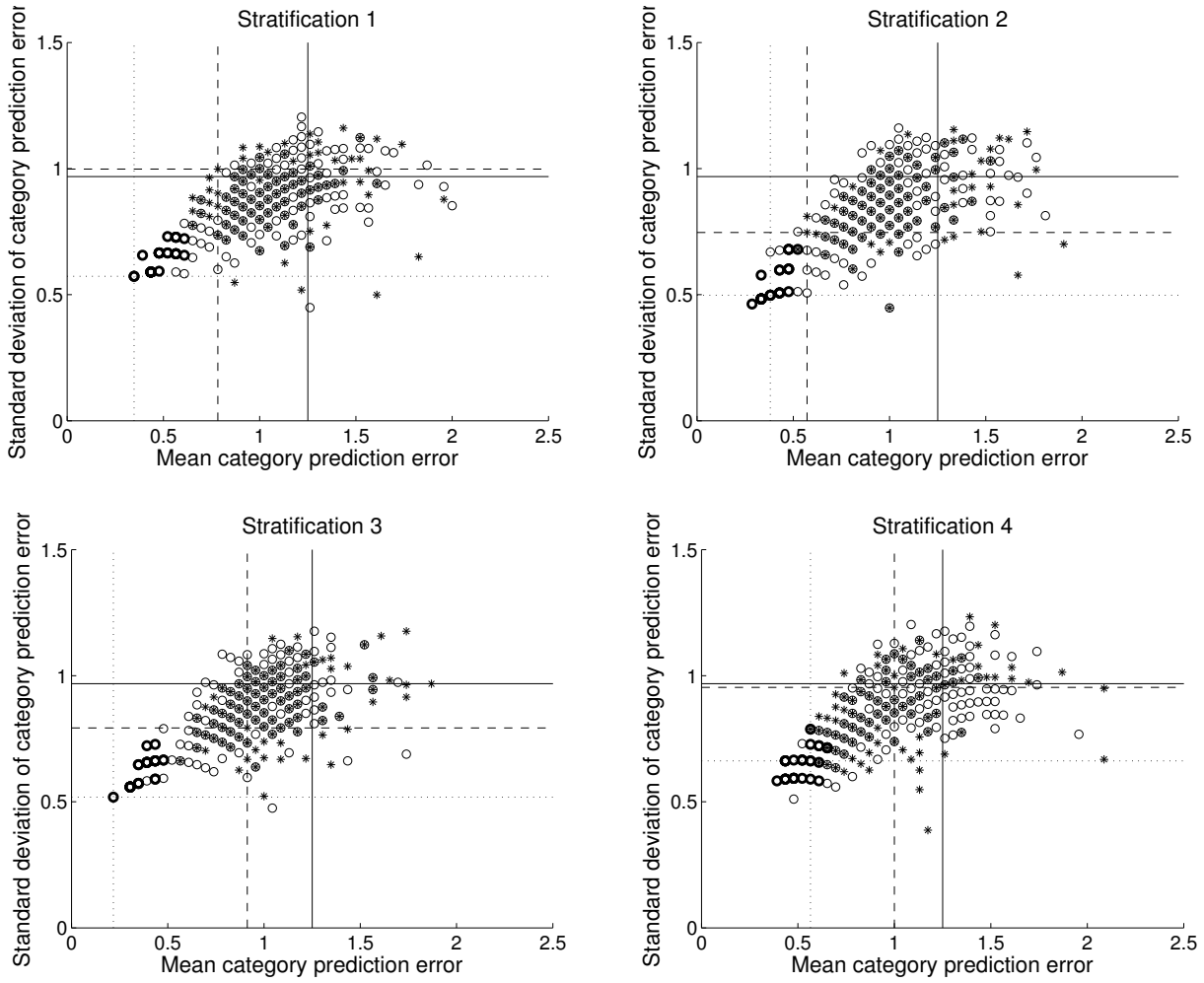

Figure S3: Scatter plot of classification error for all of the different markers for stratified datasets. The most predictive markers for the full dataset, as shown in bold in Figure 5 of the main text , are again shown here in bold for the four stratified datasets. Simulated markers from hERG-only block are denoted with '$*$' whilst multichannel block markers are denoted by '$\circ$'. Solid lines indicate the expected values if classification was performed at random, dashed lines are the values given by log10([hERG IC50]/[EFTPC High]), dotted lines are the values for the longest APD90 from simulations of Grandi *et al.*[26] at low/med/high EFTPC, it provides a consistent improvement over the existing safety factor.

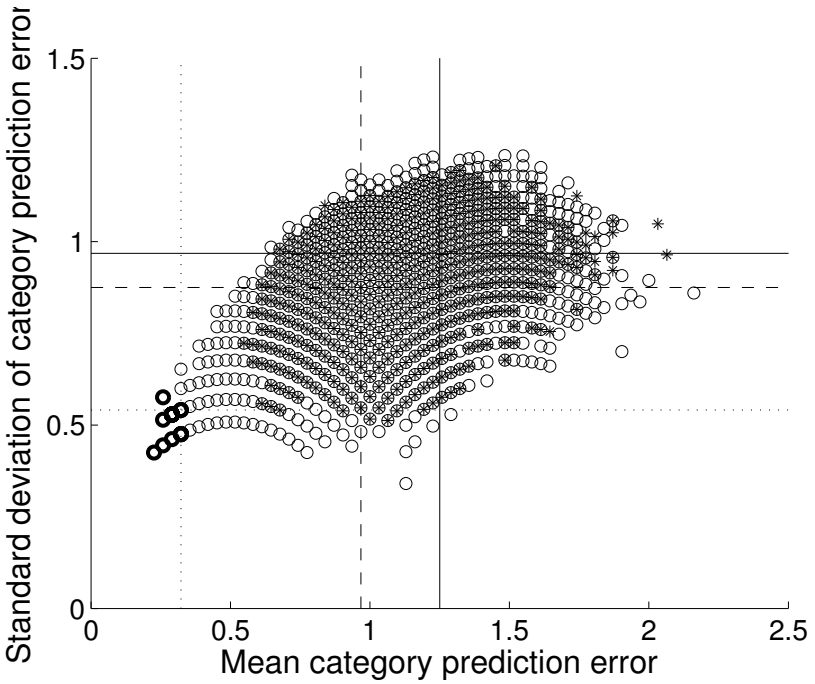

Figure S4: Scatter plot of classification error for all of the different 2D markers. Simulated markers where both are from hERG-only block are denoted with '$*$' whilst multichannel block or mixed markers are denoted by '$\circ$'. Solid lines indicate the expected values if classification was performed at random, dashed lines are the values given by log10([hERG IC50]/[high EFTPC]), dotted lines are the values given by the best 1D marker as shown in Figure 3(b) of the main text . Again, all of the 30 most predictive 2D markers result from multichannel simulations and these are denoted with bold markers.

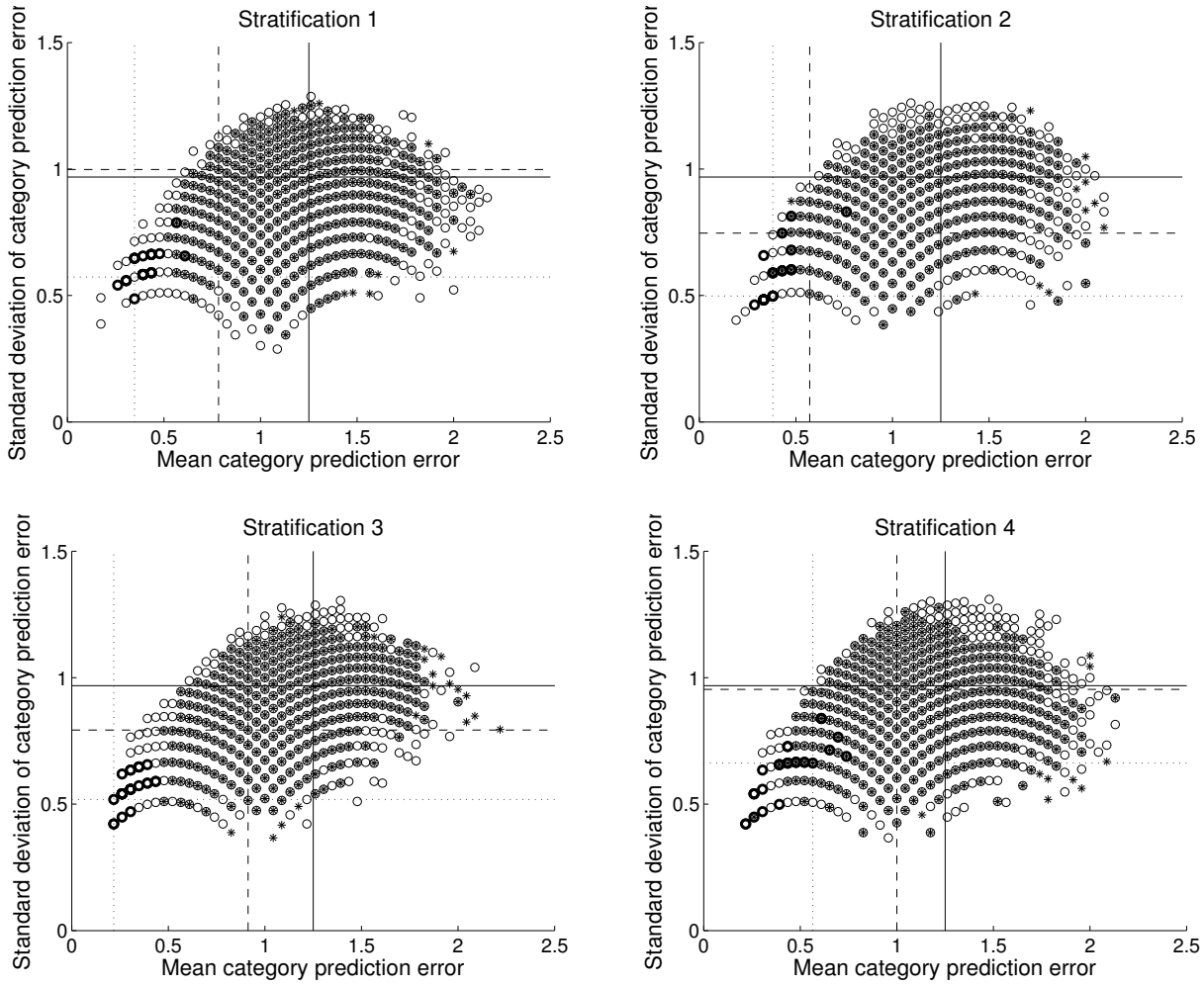

Figure S5: Scatter plot of classification error for all of the different 2D markers for stratified datasets. The most predictive markers for the full dataset, as shown in bold in Figure S4 of the main text, are again shown here in bold for the four stratified datasets. Where both simulated markers are from hERG-only block they are denoted with '$*$' whilst multichannel block or mixed markers are denoted by '$\circ$'. Solid lines indicate the expected values if classification was performed at random, dashed lines are the values given by log10([hERG IC50]/[EFTPC High]), dotted lines are the values from the 1D measure (the longest APD90 from simulations of Grandi *et al.*[26] at low/med/high EFTPC).

4 Most predictive markers

The 30 most predictive markers resulting from the LDA leave-one-out trial are shown in Table S1. Notice that all are from multi-channel block simulations, and the majority are measures associated with AP prolongation. All of these markers provide risk predictions which have less than half of the error in classification that the current best-practise marker exhibits, as shown in Figure 5 of the main text.

Error in category		Discriminant Measure
Mean	Std. Dev.	
0.323	0.541	Grandi *et al.* APD90 EFTPC with largest effect
0.355	0.551	Shannon *et al.* (2004) Peak Ca EFTPC with largest effect
0.387	0.558	Shannon *et al.* (2004) APD50 Medium EFTPC
0.387	0.615	Shannon *et al.* (2004) Dynamic EAD Start Freq EFTPC with largest effect
0.419	0.564	ten Tusscher & Panfilov (2006) APD50 Medium EFTPC
0.419	0.620	Shannon *et al.* (2004) Peak Ca High EFTPC
0.419	0.620	Shannon *et al.* (2004) Dynamic Max Slope EFTPC with largest effect
0.419	0.620	Shannon *et al.* (2004) Dynamic Area Between Curves High EFTPC
0.419	0.620	Hund & Rudy (2004) Dynamic Alternans Start Freq EFTPC with largest effect
0.419	0.620	Hund & Rudy (2004) Dynamic Instability Onset Freq EFTPC with largest effect
0.419	0.620	Grandi *et al.* (2010) Dynamic Area Between Curves Medium EFTPC
0.419	0.672	Shannon *et al.* (2004) APD50 High EFTPC
0.419	0.672	Shannon *et al.* (2004) Dynamic EAD Start Freq Medium EFTPC
0.419	0.672	Grandi *et al.* (2010) Dynamic Area Between Curves High EFTPC
0.452	0.568	Shannon *et al.* (2004) APD90 Medium EFTPC
0.452	0.568	Shannon *et al.* (2004) Peak Ca Medium EFTPC
0.452	0.568	Shannon *et al.* (2004) Dynamic Area Between Curves Medium EFTPC
0.452	0.568	Grandi *et al.* (2010) Dynamic Area Between Curves EFTPC with largest effect
0.452	0.624	Shannon *et al.* (2004) APD90 High EFTPC
0.452	0.624	Shannon *et al.* (2004) Dynamic Area Between Curves EFTPC with largest effect
0.452	0.624	ten Tusscher & Panfilov (2006) APD90 High EFTPC
0.452	0.624	ten Tusscher & Panfilov (2006) APD50 High EFTPC
0.452	0.624	ten Tusscher & Panfilov (2006) Dynamic Area Between Curves Medium EFTPC
0.452	0.624	Hund & Rudy (2004) Dynamic Instability Onset Freq Low EFTPC
0.452	0.624	Grandi *et al.* (2010) APD50 EFTPC with largest effect
0.484	0.570	Shannon *et al.* (2004) CaD90 Medium EFTPC
0.484	0.626	Shannon *et al.* (2004) APD90 EFTPC with largest effect
0.484	0.626	Shannon *et al.* (2004) APD50 EFTPC with largest effect
0.484	0.626	ten Tusscher & Panfilov (2006) APD90 Medium EFTPC
0.484	0.626	Hund & Rudy (2004) Dynamic Instability Onset Freq Medium EFTPC

Table S1: The 30 most predictive 1D measures, as highlighted in bold in Figure 5 of the main text. All are multi-channel simulated markers.

5 Classification Errors

The errors in Table S2 resulted from leave-one-out, linear discriminant analysis, when classifying according to Grandi *et al.* largest APD90 at any EFTPC.

Generic Drug Name	APD90 Change (ms)	Risk Category Actual	Risk Category Predicted	Error (categories)
Ajmaline	2.37	2	3	1
Amiodarone	0.37	2	4	2
Dofetilide	12.51	2	2	0
Quinidine	26.68	2	2	0
Tedisamil	1.40	2	3	1
Cisapride	19.71	2	2	0
Prenylamine	6.75	2	3	1
Terfenadine	18.01	2	2	0
Thioridazine	18.31	2	2	0
Bepridil	2.82	3	3	0
Chlorpromazine	1.14	3	3	0
Haloperidol	4.62	3	3	0
Pimozide	1.26	3	3	0
Sertindole	4.24	3	3	0
Amitriptyline	-0.01	4	4	0
Desipramine	-1.27	4	4	0
Diphenhydramine	0.22	4	4	0
Fluvoxamine	-0.28	4	4	0
Imipramine	-0.12	4	4	0
Mexiletine	-0.60	4	4	0
Mibefradil	-5.21	4	4	0
Nifedipine	-6.91	4	5	1
Propafenone	0.38	4	4	0
Quetiapine	-0.09	4	4	0
Cibenzoline	-0.85	5	4	1
Diltiazem	-14.36	5	5	0
Nitrendipine	-29.51	5	5	0
Phenytoin	-3.35	5	4	1
Propranolol	0.31	5	4	1
Risperidone	0.51	5	4	1
Verapamil	-20.75	5	5	0

Table S2: Classification errors resulting from use of the most predictive measure, there are compiled into a histogram to make Figure 4(d) in the main text.

6 Full list of references

1. Pratt CM, Al-Khalidi HR, Brum JM, Holroyde MJ, Schwartz PJ, Marcello SR *et al.* Cumulative experience of azimilide-associated torsades de pointes ventricular tachycardia in the 19 clinical studies comprising the azimilide database. *J Am Coll Cardiol* 2006;**48**:471–477.

2. Darpö B. Spectrum of drugs prolonging QT interval and the incidence of torsades de pointes. *Eur Heart J Supp* 2001;**3**:K70.

3. Justo D, Prokhorov V, Heller K, Zeltser D. Torsade de pointes induced by psychotropic drugs and the prevalence of its risk factors. *Acta Psychiatrica Scandinavica* 2005;**111**:171–176.

4. Bisset AF, Arshad P, Morcos M, Sridharan B. Discontinuation of thioridazine. *BMJ* 2002;**325**:967.

5. Henney JE. Withdrawal of troglitazone and cisapride. *JAMA* 2000;**283**:2228.

6. Gottlieb S. Antihistamine drug withdrawn by manufacturer. *BMJ* 1999;**319**:7.

7. Josefson D. Hay fever drug to be banned by the FDA. *BMJ* 1997;**314**:248.

8. Curran ME, Splawski I, Timothy KW, Vincen GM, Green ED, Keating MT. A molecular basis for cardiac arrhythmia: HERG mutations cause long QT syndrome. *Cell* 1995;**80**:795–803.

9. Katchman AN, Koerner J, Tosaka T, Woosley RL, Ebert SN. Comparative evaluation of HERG currents and QT intervals following challenge with suspected torsadogenic and nontorsadogenic drugs. *J Pharmacol Exp Ther* 2006;**316**:1098–1106.

10. Brugada R, Brugada J, Antzelevitch C, Kirsch GE, Potenza D, Towbin JA *et al.* Sodium channel blockers identify risk for sudden death in patients with ST-segment elevation and right bundle branch block but structurally normal hearts. *Circ* 2000;**101**:510.

11. Martin RL, McDermott JS, Salmen HJ, Palmatier J, Cox BF, Gintant GA. The utility of hERG and repolarization assays in evaluating delayed cardiac repolarization: influence of multi-channel block. *J Cardiovas Pharmacol* 2004;**43**:369–379.

12. Hoffmann P, Warner B. Are hERG channel inhibition and QT interval prolongation all there is in drug-induced torsadogenesis? A review of emerging trends. *J Pharmacol Toxicol Meth* 2006;**53**:87–105.

13. Lawrence CL, Bridgland-Taylor MH, Pollard CE, Hammond TG, Valentin JP. A rabbit Langendorff heart proarrhythmia model: predictive value for clinical identification of torsades de pointes. *Br J Pharmacol* 2006;**149**:845–860.

14. Darpo B, Nebout T, Sager PT. Clinical evaluation of QT/QTc prolongation and proarrhythmic potential for nonantiarrhythmic drugs: the International Conference on Harmonization of Technical Requirements for Registration of Pharmaceuticals for Human Use E14 guideline. *J Clin Pharmacol* 2006;**46**:498.

15. Shah RR. Drugs, QT interval prolongation and ICH E14: the need to get it right. *Drug Safety* 2005;**28**: 115–125.

16. Valentin JP, Hammond T. Safety and secondary pharmacology: successes, threats, challenges and opportunities. *J Pharmacol Toxicol Meth* 2008;**58**:77–87.

17. Redfern WS, Carlsson L, Davis AS, Lynch WG, MacKenzie I, Palethorpe S *et al.* Relationships between preclinical cardiac electrophysiology, clinical QT interval prolongation and torsade de pointes for a broad range of drugs: evidence for a provisional safety margin in drug development. *Cardiovas Res* 2003;**58**:32–45.

18. De Bruin ML, Pettersson M, Meyboom RHB, Hoes AW, Leufkens HGM. Anti-HERG activity and the risk of drug-induced arrhythmias and sudden death. *Eur Heart J* 2005;**26**:590–597.

19. Drici MD, Priori S. Cardiovascular risks of atypical antipsychotic drug treatment. *Pharmacoepidemiology and drug safety* 2007;**16**:882–890.

20. Vieweg WVR, Schneider RK, Wood MA. Torsade de pointes in a patient with complex medical and psychiatric conditions receiving low-dose quetiapine. *Acta Psychiatrica Scandinavica* 2005;**112**:318–322.

21. Powell T. The isolation and characterization of calcium-tolerant myocytes. *Basic Res Cardiol* 1985;**80**:15.

22. Shannon TR, Wang F, Puglisi J, Weber C, Bers DM. A mathematical treatment of integrated Ca dynamics within the ventricular myocyte. *Biophys J* 2004;**87**:3351–3371.

23. Mahajan A, Shiferaw Y, Sato D, Baher A, Olcese R, Xie LH *et al.* A rabbit ventricular action potential model replicating cardiac dynamics at rapid heart rates. *Biophys J* 2008;**94**:392–410.

24. Hund TJ, Rudy Y. Rate dependence and regulation of action potential and calcium transient in a canine cardiac ventricular cell model. *Circ* 2004;**110**:3168–3174.

25. Ten Tusscher K, Panfilov AV. Alternans and spiral breakup in a human ventricular tissue model. *Am J Physiol Heart Circ Physiol* 2006;**291**:1088–1100.

26. Grandi E, Pasqualini FS, Bers DM. A novel computational model of the human ventricular action potential and Ca transient. *J Mol Cellular Cardiology* 2010;**48**:112–121.

27. Brennan T, Fink M, Rodriguez B. Multiscale modelling of drug-induced effects on cardiac electrophysiological activity. *Eur J Pharmaceut Sci* 2009;**36**:62–77.

28. Lloyd CM, Lawson JR, Hunter PJ, Nielsen PF. The CellML model repository. *Bioinformatics* 2008;**24**: 2122–2123.

29. Garny A, Nickerson DP, Cooper J, Santos RW, Miller AK, McKeever S *et al.* CellML and associated tools and techniques. *Phil Trans R Soc A* 2008;**366**:3017–3043.

30. Hindmarsh AC, Brown PN, Grant KE, Lee SL, Serban R, Shumaker DE *et al.* SUNDIALS: Suite of nonlinear and differential/algebraic equation solvers. *ACM Trans Math Software (TOMS)* 2005;**31**:363–396.

31. Pitt-Francis J, Pathmanathan P, Bernabeu MO, Bordas R, Cooper J, Fletcher AG *et al.* Chaste: A test-driven approach to software development for biological modelling. *Comp Phys Comm* 2009;**180**:2452–2471.

32. Noble D. Cardiac action and pacemaker potentials based on the Hodgkin-Huxley equations. *Nature* 1960; **188**:495–497.

33. Shah RR, Hondeghem LM. Refining detection of drug-induced proarrhythmia: QT interval and TRIaD. *Heart Rhythm* 2005;**2**:758–772.

34. Bahnikova M, Matejovic P, Pasek M, Simurda J. Ajmaline-induced block of sodium current in rat ventricular myocytes. *Scripta Medica (Brno)* 2002;**75**:169–178.

35. Bébarová M, Matejovic P, Pásek M, Simurdova M, Simurda J. Effect of ajmaline on action potential and ionic currents in rat ventricular myocytes. *General Physiology and Biophysics* 2005;**24**:311–325.

36. Kiesecker C, Zitron E, Lück S, Bloehs R, Scholz EP, Kathöfer S *et al.* Class Ia anti-arrhythmic drug ajmaline blocks HERG potassium channels: mode of action. *Naunyn-Schmiedeberg's archives of pharmacology* 2004; **370**:423–435.

37. Köppel C, Oberdisse U, Heinemeyer G. Clinical course and outcome in class IC antiarrhythmic overdose. *Clinical Toxicology* 1990;**28**:433–444.

38. Grima M, Schwartz J, Spach MO, Velly J. Anti-anginal arylalkylamines and sodium channels:[3H]-batrachotoxinin-A 20-alpha-benzoate and [3H]-tetracaine binding. *British journal of pharmacology* 1986; **89**:641–646.

39. Lubic SP, Nguyen KPV, Dave B, Giacomini JC. Antiarrhythmic agent amiodarone possesses calcium channel blocker properties. *Journal of Cardiovascular Pharmacology* 1994;**24**:707–714.

40. Leffler A, Reiprich A, Mohapatra DP, Nau C. Use-dependent block by lidocaine but not amitriptyline is more pronounced in tetrodotoxin (TTX)-Resistant Nav1. 8 than in TTX-sensitive Na+ channels. *J Pharmacol Exp Ther* 2007;**320**:354–364.

41. Zahradník I, Minarovič I, Zahradníková A. Inhibition of the cardiac L-type calcium channel current by antidepressant drugs. *J Pharmacol Exp Ther* 2008;**324**:977–984.

42. Jo SH, Youm JB, Lee CO, Earm YE, Ho WK. Blockade of the HERG human cardiac K+ channel by the antidepressant drug amitriptyline. *British journal of pharmacology* 2000;**129**:1474–1480.

43. Fossa AA, DePasquale MJ, Raunig DL, Avery MJ, Leishman DJ. The Relationship of Clinical QT Prolongation to Outcome in the Conscious Dog Using a Beat-to-Beat QT-RR Interval Assessment. *J Pharmacol Exp Ther* 2002;**302**:828–833.

44. McNeal ET, Lewandowski GA, Daly JW, Creveling CR. [3H] Batrachotoxinin A 20 alpha-benzoate binding

to voltage-sensitive sodium channels: a rapid and quantitative assay for local anesthetic activity in a variety of drugs. *J Med Chem* 1985;**28**:381–388.

45. Testa R, Abbiati G, Ceserani R, Restelli G, Vanasia A, Barone D *et al.* Profile of in vitro binding affinities of neuroleptics at different rat brain receptors: cluster analysis comparison with pharmacological and clinical profiles. *Pharmaceutical research* 1989;**6**:571–577.

46. Leong Max K. A novel approach using pharmacophore ensemble/support vector machine (phe/svm) for prediction of herg liability. *Chemical Research in Toxicology* 2007;**20**:217–226.

47. Sato T, Wu B, Kiyosue T, Arita M. Effects of cibenzoline, a new class Ia antiarrhythmic drug, on various membrane ionic currents and action potentials of guinea-pig ventricular cells. *Naunyn-Schmiedeberg's archives of pharmacology* 1994;**350**:167–173.

48. Matsuoka S, Nawada T, Hisatome I, Miyamoto J, Hasegawa J, Kotake H *et al.* Comparison of Ca2+ channel inhibitory effects of cibenzoline with verapamil on guinea-pig heart. *General Pharmacology: The Vascular System* 1991;**22**:87–91.

49. Männikkö R, Overend G, Perrey C, Gavaghan CL, Valentin JP, Morten J *et al.* Pharmacological and electrophysiological characterization of nine, single nucleotide polymorphisms of the hERG-encoded potassium channel. *Br J Pharmacol* 2010;**159**:102–114.

50. Mohammad S, Zhou Z, Gong Q, January CT. Blockage of the HERG human cardiac K+ channel by the gastrointestinal prokinetic agent cisapride. *American Journal of Physiology- Heart and Circulatory Physiology* 1997;**273**:H2534–H2538.

51. Ekins S, Crumb WJ, Sarazan RD, Wikel JH, Wrighton SA. Three-dimensional quantitative structure-activity relationship for inhibition of human ether-a-go-go-related gene potassium channel. *J Pharmacol Exp Ther* 2002;**301**:427–434.

52. Pauwels PJ, Laduron PM. TPP+ accumulation in rat brain synaptosomes as a probe for Na+ channels. *European journal of pharmacology* 1986;**132**:289–293.

53. Dohmoto H, Takahara A, Uneyama H, Yoshimoto R. Cardiac Ca 2+ Channel-Blocking Effects of the Cyproheptadine Derivative AH-1058 in Isolated Guinea Pig Cardiomyocytes. *Journal of pharmacological sciences* 2003;**91**:163–166.

54. Campiani G, Fiorini I, De Filippis MP, Ciani SM, Garofalo A, Nacci V *et al.* Cardiovascular characterization of pyrrolo [2, 1-d][1, 5] benzothiazepine derivatives binding selectively to the peripheral-type benzodiazepine receptor (PBR): from dual PBR affinity and calcium antagonist activity to novel and selective calcium entry blockers. *J Med Chem* 1996;**39**:2922–2938.

55. Zhang S, Zhou Z, Gong Q, Makielski JC, January CT. Mechanism of block and identification of the verapamil binding domain to HERG potassium channels. *Circulation research* 1999;**84**:989–998.

56. Johnson RE, Silver PJ, Becker R, Birsner NC, Bohnet EA, Briggs GM *et al.* 4, 5-Dihydro-3-(methanesulfonamidophenyl)-1-phenyl-1H-2, 4-benzodiazepines: A novel class III antiarrhythmic agents. *Journal of medicinal chemistry* 1995;**38**:2551–2556.

57. Chadwick CC, Ezrin AM, O'Connor B, Volberg WA, Smith DI, Wedge KJ *et al.* Identification of a specific radioligand for the cardiac rapidly activating delayed rectifier K+ channel. *Circulation research* 1993;**72**: 707–714.

58. DeVane CL. Metabolism and pharmacokinetics of selective serotonin reuptake inhibitors. *Cellular and molecular neurobiology* 1999;**19**:443–466.

59. Schoemaker H, Claustre Y, Fage D, Rouquier L, Chergui K, Curet O *et al.* Neurochemical characteristics of amisulpride, an atypical dopamine D2/D3 receptor antagonist with both presynaptic and limbic selectivity. *J Pharmacol Exp Therap* 1997;**280**:83–97.

60. Kirsch GE, Trepakova ES, Brimecombe JC, Sidach SS, Erickson HD, Kochan MC *et al.* Variability in the measurement of hERG potassium channel inhibition: effects of temperature and stimulus pattern. *Journal of pharmacological and toxicological methods* 2004;**50**:93–101.

61. De Luca A, Talon S, De Bellis M, Desaphy JF, Franchini C, Lentini G *et al.* Inhibition of skeletal muscle sodium currents by mexiletine analogues: specific hydrophobic interactions rather than lipophilia per se account for drug therapeutic profile. *Naunyn-Schmiedeberg's archives of pharmacology* 2003;**367**:318–327.

62. Hu XD, Qian JQ, Agents AA, Separation C, Pigs G, Cells M *et al.* DDPH inhibited L-type calcium current and sodium current in a single ventricular myocyte of guinea pig. *Acta pharmacologica Sinica* 2001;**22**: 415–419.

63. Roche O, Trube G, Zuegge J, Pflimlin P, Alanine A, Schneider G. A virtual screening method for prediction of the hERG potassium channel liability of compound libraries. *ChemBioChem* 2002;**3**:455–459.

64. Strege PR, Bernard CE, Ou Y, Gibbons SJ, Farrugia G. Effect of mibefradil on sodium and calcium currents. *American Journal of Physiology- Gastrointestinal and Liver Physiology* 2005;**289**:249–253.

65. Huber I, Wappl E, Herzog A, Mitterdorfer J, Glossmann H, Langer T *et al.* Conserved Ca2+-antagonist-binding properties and putative folding structure of a recombinant high-affinity dihydropyridine-binding domain. *Biochemical Journal* 2000;**347**:829–836.

66. Di Stilo A, Visentin S, Cena C, Gasco AM, Ermondi G, Gasco A. New 1, 4-dihydropyridines conjugated to furoxanyl moieties, endowed with both nitric oxide-like and calcium channel antagonist vasodilator activities. *J Med Chem* 1998;**41**:5393–5401.

67. Zhabyeyev P, Missan S, Jones SE, McDonald TF. Low-affinity block of cardiac K+ currents by nifedipine. *European journal of pharmacology* 2000;**401**:137–143.

68. Ehlert FJ, Roeske WR, Itoga E, Yamamura HI. The binding of [3H] nitrendipine to receptors for calcium channel antagonists in the heart, cerebral cortex, and ileum of rats. *Life Sciences* 1982;**30**:2191–2202.

69. Pauwels PJ, Leysen JE, Laduron PM. [3H] Batrachotoxinin a 20-[alpha]-benzoate binding to sodium channels in rat brain: Characterization and pharmacological significance. *European journal of pharmacology* 1986;**124**:291–298.

70. Reynolds IJ, Snowman AM, Snyder SH. (-)-[3H] desmethoxyverapamil labels multiple calcium channel modulator receptors in brain and skeletal muscle membranes: differentiation by temperature and dihydropyridines. *J Pharmacol Exp Ther* 1986;**237**:731–738.

71. Gietl Y, Spahn H, Knauf H, Mutschler E. Single-and multiple-dose pharmacokinetics of R-(-)-and S-(+)-prenylamine in man. *Eur J Clin Pharmacol* 1990;**38**:587–593.

72. Paul AA, Witchel HJ, Hancox JC. Inhibition of the current of heterologously expressed HERG potassium channels by flecainide and comparison with quinidine, propafenone and lignocaine. *British Journal of Pharmacology* 2002;**136**:717–729.

73. Hanson LA, Bass AS, Gintant G, Mittelstadt S, Rampe D, Thomas K. ILSI-HESI cardiovascular safety subcommittee initiative: evaluation of three non-clinical models of QT prolongation. *Journal of pharmacological and toxicological methods* 2006;**54**:116–129.

74. Pine M, Favrot L, Smith S, McDonald K, Chidsey CA. Correlation of plasma propranolol concentration with therapeutic response in patients with angina pectoris. *Circulation* 1975;**52**:886.

75. Kongsamut S, Kang J, Chen XL, Roehr J, Rampe D. A comparison of the receptor binding and HERG channel affinities for a series of antipsychotic drugs. *European journal of pharmacology* 2002;**450**:37–41.

76. Po SS, Wang DW, Yang ICH, Johnson Jr JP, Nie L, Bennett PB. Modulation of HERG potassium channels by extracellular magnesium and quinidine. *Journal of cardiovascular pharmacology* 1999;**33**:181.

77. Thomsen MB, Volders PGA, Stengl M, Späatjens RL, Beekman JDM, Bischoff U *et al.* Electrophysiological safety of sertindole in dogs with normal and remodeled hearts. *J Pharmacol Exp Ther* 2003;**307**:776–784.

78. Faivre JF, Gout B, Bril A. Tedisamil. *Cardiovascular Drug Reviews* 1995;**13**:33–50.

79. Jost N, Virag L, Hala O, Varro A, Thormahlen D, Papp JG. Effect of the antifibrillatory compound tedisamil (KC-8857) on transmembrane currents in mammalian ventricular myocytes. *Current medicinal chemistry* 2004;**11**:3219–3228.

80. Hastie T, Tibshirani R, Friedman JH. *The elements of statistical learning: data mining, inference, and prediction*. Springer New York, 2nd edition, 2009.